PHOTONICS Research

Quantum information transfer between a two-level and a four-level quantum systems

Tianfeng Feng,[1,†] Qiao Xu,[1,†] Linxiang Zhou,[1,†] Maolin Luo,[1] Wuhong Zhang,[1,2] and Xiaoqi Zhou[1,*]

[1]State Key Laboratory of Optoelectronic Materials and Technologies and School of Physics, Sun Yat-sen University, Guangzhou 510275, China
[2]Department of Physics, Jiujiang Research Institute and Collaborative Innovation Center for Optoelectronic Semiconductors and Efficient Devices, Xiamen University, Xiamen 361005, China
*Corresponding author: zhouxq8@mail.sysu.edu.cn

Received 20 April 2022; revised 5 October 2022; accepted 13 October 2022; posted 14 October 2022 (Doc. ID 461283); published 30 November 2022

Quantum mechanics provides a disembodied way to transfer quantum information from one quantum object to another. In theory, this quantum information transfer can occur between quantum objects of any dimension, yet the reported experiments of quantum information transfer to date have mainly focused on the cases where the quantum objects have the same dimension. Here, we theoretically propose and experimentally demonstrate a scheme for quantum information transfer between quantum objects of different dimensions. By using an optical qubit-ququart entangling gate, we observe the transfer of quantum information between two photons with different dimensions, including the flow of quantum information from a four-dimensional photon to a two-dimensional photon and vice versa. The fidelities of the quantum information transfer range from 0.700 to 0.917, all above the classical limit of 2/3. Our work sheds light on a new direction for quantum information transfer and demonstrates our ability to implement entangling operations beyond two-level quantum systems.

https://doi.org/10.1364/PRJ.461283

1. INTRODUCTION

The information transfer between different objects is one of the most fundamental phenomena in nature. In the classical world, a macroscopic object that carries unknown information can have its information precisely measured and copied, and thus this information can be transferred to another object while still being retained on the original object. In the quantum world, although quantum mechanics does not allow the unknown quantum information carried on a quantum object to be perfectly cloned or precisely measured [1,2], it does allow quantum information to be transferred from one object to another object in a disembodied way, i.e., only the quantum information but not the object itself is transferred. Quantum information transfer (QIT) between two quantum objects, which is also called quantum teleportation [3,4] when the two objects are separated at different locations, is widely used in quantum information applications including long-distance quantum communication [5–7], distributed quantum networks [8,9], and measurement-based quantum computation [10–14]. It has been experimentally demonstrated in a variety of physical systems [15–27], including photons [17,18], atoms [19], ions [20–22], electrons [23], defects in solid states [24], optomechanical systems [25], and superconducting circuits [26,27]. Recently, more complex experiments have also been reported, such as the open destination teleportation [28,29] and the teleportation of a composite system [30,32], a multilevel state [31,32], and multidegree of freedom of a particle [33].

So far, the reported experiments have mainly focused on QIT between quantum objects with the same dimension. However, in quantum applications such as distributed quantum networks, different quantum objects may have different dimensions, and QIT between them is also required. For example, as shown in Fig. 1(a), there are two quantum objects A and B, where A is two-dimensional (2D) and carries no quantum information, and B is four-dimensional (4D) and carries two qubits of unknown quantum information beforehand. If B wants to transfer quantum information to A, because A is 2D and capable of carrying at most one qubit of quantum information, only one of the two qubits stored in B can be transferred to A. We call this process a 4-to-2 QIT, which will distribute the two qubits of quantum information originally concentrated on B over both A and B. Now A and B are each loaded with one qubit of quantum information. Obviously, as shown in Fig. 1(b), this one qubit of quantum information stored in A can also be transferred back to B. We call this process a 2-to-4 QIT, which concentrates the two qubits of quantum information distributed over both A and B on object B only.

In this work, we theoretically propose and experimentally demonstrate a scheme for QIT between a 2D quantum object and a 4D one. By using an optical qubit-ququart entangling gate, we successfully transfer one qubit of quantum information

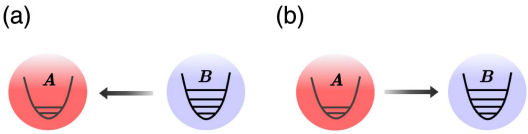

Fig. 1. Quantum information transfer between a two-level and a four-level quantum systems. (a) Quantum information transfer from a four-level system B to a two-level system A. (b) Quantum information transfer from a two-level system A to a four-level system B.

from a 4D photon preloaded with two qubits of quantum information to a 2D photon, i.e., achieving a 4-to-2 QIT. We also experimentally realize a 2-to-4 QIT, i.e., transferring one qubit of quantum information from a 2D photon to a 4D photon preloaded with one qubit of quantum information. Besides fundamental interests, the QITs demonstrated here have the potential to simplify the construction of quantum circuits and find applications in quantum computation and quantum communications.

2. SCHEME OF QUANTUM INFORMATION TRANSFER

A. 2-to-2 QIT

Before presenting the scheme for implementing the QIT between quantum objects of different dimensions, let us briefly review how to implement the QIT between quantum objects of the same dimensions. Here we take the 2D case as an example, assuming that both A and B are 2D quantum objects, where A is in the state $\frac{1}{\sqrt{2}}(|\mathbf{0}\rangle_A + |\mathbf{1}\rangle_A)$ without any quantum information preloaded, and B is in the state $\alpha|\mathbf{0}\rangle_B + \beta|\mathbf{1}\rangle_B$ loaded with one-qubit unknown quantum information. As shown in Fig. 2(a), by applying a controlled-X gate (CX gate, commonly referred as CNOT gate) on A and B, the quantum state of the composite system of A and B would become

$$\frac{1}{\sqrt{2}}|\mathbf{0}\rangle_A(\alpha|\mathbf{0}\rangle_B + \beta|\mathbf{1}\rangle_B) + \frac{1}{\sqrt{2}}|\mathbf{1}\rangle_A(\alpha|\mathbf{1}\rangle_B + \beta|\mathbf{0}\rangle_B)$$
$$= \frac{1}{\sqrt{2}}(\alpha|\mathbf{0}\rangle_A + \beta|\mathbf{1}\rangle_A)|\mathbf{0}\rangle_B + \frac{1}{\sqrt{2}}(\beta|\mathbf{0}\rangle_A + \alpha|\mathbf{1}\rangle_A)|\mathbf{1}\rangle_B,$$

where $X|\mathbf{0}\rangle = |\mathbf{1}\rangle, X|\mathbf{1}\rangle = |\mathbf{0}\rangle$. After measuring B in the $|\mathbf{0}/\mathbf{1}\rangle$ basis and forwarding the measurement outcome to A, a unitary operation (I or X) based on the outcome is applied on A and thus converts its state to $\alpha|\mathbf{0}\rangle_A + \beta|\mathbf{1}\rangle_A$. The state of A now has the same form as the initial state of B and thus completes the QIT from B to A.

B. 4-to-2 QIT

We now present the scheme for realizing the QIT from a 4D to a 2D quantum object. Suppose A is still 2D and in the state $\frac{1}{\sqrt{2}}(|\mathbf{0}\rangle_A + |\mathbf{1}\rangle_A)$, and B is now 4D and in the state

$$\alpha|\mathbf{0}\rangle_B + \beta|\mathbf{1}\rangle_B + \gamma|\mathbf{2}\rangle_B + \delta|\mathbf{3}\rangle_B, \quad \textbf{(1)}$$

which is preloaded with two-qubit unknown quantum information. To achieve the QIT between a 2D and a 4D quantum object, instead of using a two-qubit gate like the CNOT gate, one should use a qubit-ququart entangling gate. As shown in

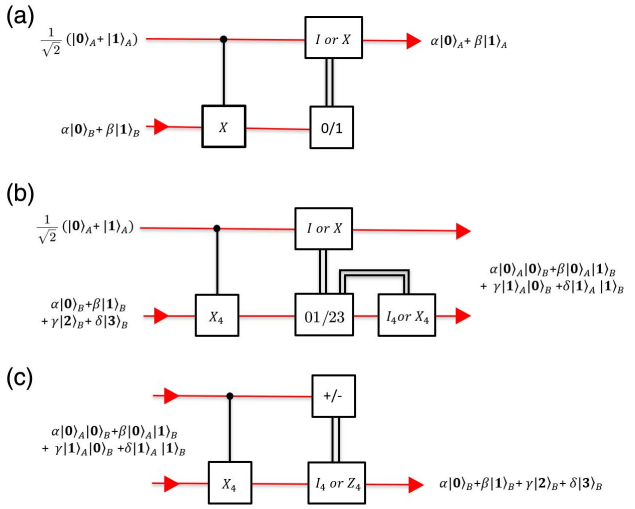

Fig. 2. Schematic diagrams for quantum information transfer. (a) The quantum information transfer from one qubit to another. The CX gate entangles qubit A, which initially contains no quantum information, and qubit B, which initially contains one qubit of unknown quantum information. The projective measurement on B removes quantum information from B, thus transferring the one qubit of quantum information to A. After the feedforward unitary operation, the quantum information originally stored in B is restored in A, thus completing the quantum information transfer. (b) The quantum information transfer from a ququart to a qubit. The initial state of ququart B contains two qubits of unknown quantum information, while qubit A initially contains no quantum information. After entangling A and B using a CX_4 gate, where X_4 swaps $|0\rangle$ and $|2\rangle$ ($|1\rangle$ and $|3\rangle$), a projective measurement is applied on B to measure whether it is in the subspace spanned by $|0\rangle$ and $|1\rangle$ or the subspace spanned by $|2\rangle$ and $|3\rangle$. Based on the measurement result, feedforward unitary operations are applied on A and B, and the final state of A and B contains the two qubits of quantum information originally stored in B, thus completing the quantum information transfer from ququart B to qubit A. (c) The quantum information transfer from a qubit to a ququart. Two qubits of unknown quantum information are initially distributed over qubit A and ququart B. After applying a CX_4 gate on A and B, a projective measurement is applied on A and a feedforward unitary operation based on the measurement result is applied on B. The final state of B contains the two qubits of quantum information originally distributed over both A and B, thus completing the quantum information transfer from qubit A to ququart B.

Fig. 2(b), a controlled-X_4 gate (CX_4) is applied to A and B, where X_4 is a 4D unitary gate defined as

$$X_4 = \begin{pmatrix} 0 & 0 & 1 & 0 \\ 0 & 0 & 0 & 1 \\ 1 & 0 & 0 & 0 \\ 0 & 1 & 0 & 0 \end{pmatrix},$$

which converts $|\mathbf{0}\rangle$ ($|\mathbf{1}\rangle$) to $|\mathbf{2}\rangle$ ($|\mathbf{3}\rangle$) and vice versa. The state of A and B is thus converted to

$$\frac{1}{\sqrt{2}}|\mathbf{0}\rangle_A(\alpha|\mathbf{0}\rangle_B+\beta|\mathbf{1}\rangle_B+\gamma|\mathbf{2}\rangle_B+\delta|\mathbf{3}\rangle_B)$$
$$+\frac{1}{\sqrt{2}}|\mathbf{1}\rangle_A(\alpha|\mathbf{2}\rangle_B+\beta|\mathbf{3}\rangle_B+\gamma|\mathbf{0}\rangle_B+\delta|\mathbf{1}\rangle_B)$$
$$=\frac{1}{\sqrt{2}}(\alpha|\mathbf{0}\rangle_A|\mathbf{0}\rangle_B+\beta|\mathbf{0}\rangle_A|\mathbf{1}\rangle_B+\gamma|\mathbf{1}\rangle_A|\mathbf{0}\rangle_B+\delta|\mathbf{1}\rangle_A|\mathbf{1}\rangle_B)$$
$$+\frac{1}{\sqrt{2}}(\alpha|\mathbf{1}\rangle_A|\mathbf{2}\rangle_B+\beta|\mathbf{1}\rangle_A|\mathbf{3}\rangle_B+\gamma|\mathbf{0}\rangle_A|\mathbf{2}\rangle_B+\delta|\mathbf{0}\rangle_A|\mathbf{3}\rangle_B).$$

A projective measurement is then applied on B to measure whether it is in the subspace spanned by $|\mathbf{0}\rangle_B$ and $|\mathbf{1}\rangle_B$ or the subspace spanned by $|\mathbf{2}\rangle_B$ and $|\mathbf{3}\rangle_B$. Based on the measurement outcome, unitary operations ($I\otimes I_4$ or $X\otimes X_4$) are applied on A and B and their state becomes

$$\alpha|\mathbf{0}\rangle_A|\mathbf{0}\rangle_B+\beta|\mathbf{0}\rangle_A|\mathbf{1}\rangle_B+\gamma|\mathbf{1}\rangle_A|\mathbf{0}\rangle_B+\delta|\mathbf{1}\rangle_A|\mathbf{1}\rangle_B, \quad (2)$$

where

$$I_4=\begin{pmatrix}1&0&0&0\\0&1&0&0\\0&0&1&0\\0&0&0&1\end{pmatrix}.$$

Comparing Eq. (2) with Eq. (1), it is observed that the two quantum states have exactly the same form except for the difference in the state basis, which means that the two-qubit quantum information previously stored in B is now distributed over both A and B. In other words, one of the two qubits of quantum information originally stored in B is now transferred to A, thus achieving a 4-to-2 QIT.

C. 2-to-4 QIT

We now show how the same quantum circuit can be used to implement a 2-to-4 QIT (the inverse of the above process), i.e., transferring one qubit of quantum information from a 2D quantum object to a 4D quantum object preloaded with one-qubit unknown quantum information. The initial state of A and B can be written as

$$\alpha|\mathbf{0}\rangle_A|\mathbf{0}\rangle_B+\beta|\mathbf{0}\rangle_A|\mathbf{1}\rangle_B+\gamma|\mathbf{1}\rangle_A|\mathbf{0}\rangle_B+\delta|\mathbf{1}\rangle_A|\mathbf{1}\rangle_B, \quad (3)$$

where both the 2D A and the 4D B are preloaded with one qubit of unknown quantum information. Note that the quantum state of A and B can be either an entangled state or a separable state. As shown in Fig. 2(c), a CX_4 gate is applied to A and B, and their state is thus converted to

$$\alpha|\mathbf{0}\rangle_A|\mathbf{0}\rangle_B+\beta|\mathbf{0}\rangle_A|\mathbf{1}\rangle_B+\gamma|\mathbf{1}\rangle_A|\mathbf{2}\rangle_B+\delta|\mathbf{1}\rangle_A|\mathbf{3}\rangle_B$$
$$=|+\rangle_A(\alpha|\mathbf{0}\rangle_B+\beta|\mathbf{1}\rangle_B+\gamma|\mathbf{2}\rangle_B+\delta|\mathbf{3}\rangle_B)$$
$$+|-\rangle_A(\alpha|\mathbf{0}\rangle_B+\beta|\mathbf{1}\rangle_B-\gamma|\mathbf{2}\rangle_B-\delta|\mathbf{3}\rangle_B),$$

where $|\pm\rangle=1/\sqrt{2}(|\mathbf{0}\rangle\pm|\mathbf{1}\rangle)$. Similarly, after measuring A in the $|\pm\rangle$ basis and forwarding the outcome to B, a 4D unitary operation (I_4 or Z_4) is applied on B conditioned on the outcome and thus converts its state to

$$\alpha|\mathbf{0}\rangle_B+\beta|\mathbf{1}\rangle_B+\gamma|\mathbf{2}\rangle_B+\delta|\mathbf{3}\rangle_B, \quad (4)$$

where

$$Z_4=\begin{pmatrix}1&0&0&0\\0&1&0&0\\0&0&-1&0\\0&0&0&-1\end{pmatrix}.$$

Comparing Eq. (4) with Eq. (3), it is observed that the two quantum states have exactly the same form except for the difference in the state basis, which means that the two qubits of quantum information previously distributed over both A and B are now concentrated in B. In other words, the one-qubit quantum information originally stored in A is now transferred to B, thus achieving a 2-to-4 QIT.

3. EXPERIMENTAL DEMONSTRATION USING LINEAR OPTICS

A. Optical CX_4 Gate

To experimentally implement the QIT operations described above, the main challenge lies in the realization of the key part of the quantum circuit, namely the qubit-ququart entangling gate CX_4. Most experimentally realized quantum entangling gates so far are based on qubits [34–40], and it is a challenging task to implement such high-dimensional entangling operations in any physical system.

Here we present our method of implementing the CX_4 gate using linear optics. As shown in Fig. 3(a), instead of implementing the CX_4 gate directly, we first decompose it into two consecutive gates CX_{02} and CX_{13} based on the fact that $X_4=X_{13}X_{02}$, where

$$X_{02}=\begin{pmatrix}0&0&1&0\\0&1&0&0\\1&0&0&0\\0&0&0&1\end{pmatrix},\quad X_{13}=\begin{pmatrix}1&0&0&0\\0&0&0&1\\0&0&1&0\\0&1&0&0\end{pmatrix}.$$

Although X_{02} (X_{13}) is a 4D unitary operation, it only operates on a 2D subspace spanned by $|\mathbf{0}\rangle$ and $|\mathbf{2}\rangle$ ($|\mathbf{1}\rangle$ and $|\mathbf{3}\rangle$). X_{02} (X_{13}) swaps $|\mathbf{0}\rangle$ and $|\mathbf{2}\rangle$ ($|\mathbf{1}\rangle$ and $|\mathbf{3}\rangle$) and leaves $|\mathbf{1}\rangle$ and $|\mathbf{3}\rangle$ ($|\mathbf{0}\rangle$ and $|\mathbf{2}\rangle$) unchanged. Based on this fact, two optical CNOT gates can be used to implement CX_{02} and CX_{13}.

As shown in Fig. 3(a), system A consists of two photons, $a1$ and $a2$, serving as the control qubit, and system B consists of photon b, serving as the target ququart. The two orthonormal basis states of system A are $|\mathbf{0}\rangle_A=|H\rangle_{a1}|H\rangle_{a2}$ and $|\mathbf{1}\rangle_A=|V\rangle_{a1}|V\rangle_{a2}$, where H and V denote horizontal and vertical polarizations, respectively. For system B, to encode a ququart with a single photon, photon b, both the polarization and spatial degrees of freedom are used, and the four orthonormal basis states are $|\mathbf{0}\rangle_B=|H0\rangle_b$, $|\mathbf{1}\rangle_B=|H1\rangle_b$, $|\mathbf{2}\rangle_B=|V0\rangle_b$, and $|\mathbf{3}\rangle_B=|V1\rangle_b$, where $H0$ ($H1$) denotes photon in the upper (lower) spatial mode with horizontal polarization, and $V0$ ($V1$) denotes photon in the upper (lower) spatial mode with vertical polarization. The CX_{02} operation between qubit A and ququart B can be realized by applying a polarization CNOT gate to photon $a1$ and photon b in the upper path, which can be understood as follows. When the polarization of photon $a1$ is H (namely qubit A in $|\mathbf{0}\rangle_A$), nothing happens; when the polarization of photon a is V (namely qubit A in $|\mathbf{1}\rangle_A$), the polarization of photon b flips between H and V if b is in the upper path (namely ququart B's $|\mathbf{0}\rangle_B$ and $|\mathbf{2}\rangle_B$ components being swapped), and is unaffected if b is in the lower path (namely ququart B's $|\mathbf{1}\rangle_B$ and $|\mathbf{3}\rangle_B$ components being unchanged), which is exactly what a CX_{02} gate achieves. Similarly, the CX_{13} operation can be realized by applying a polarization CNOT gate to photon $a2$ and photon b in the

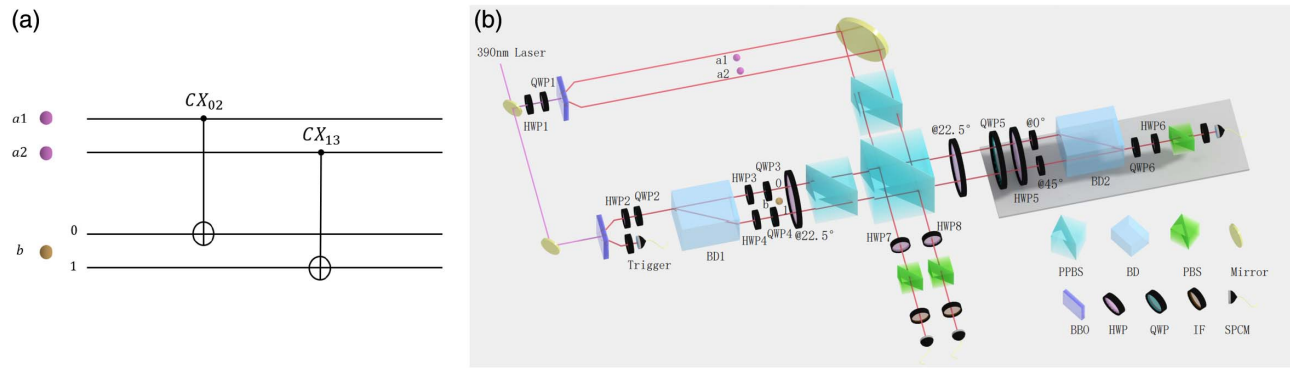

Fig. 3. Experimental layout for quantum information transfer between a qubit and a ququart. (a) Optical CX_4 gate. Two photons $a1$ and $a2$ are used to encode qubit A, where $|\mathbf{0}\rangle_A = |H\rangle_{a1}|H\rangle_{a2}$ and $|\mathbf{1}\rangle_A = |V\rangle_{a1}|V\rangle_{a2}$. Photon b is used to encode ququart B, where $|\mathbf{0}\rangle_B = |H0\rangle_b$, $|\mathbf{1}\rangle_B = |H1\rangle_b$, $|\mathbf{2}\rangle_B = |V0\rangle_b$, and $|\mathbf{3}\rangle_B = |V1\rangle_b$. $H0$ ($H1$) denotes photon in the upper (lower) spatial mode with horizontal polarization and $V0$ ($V1$) denotes photon in upper (lower) spatial mode with vertical polarization. A CX_4 gate between the control qubit A and the target ququart B is decomposed into a CX_{02} gate and a CX_{13} gate. The CX_{02} (CX_{13}) gate is equivalent to a polarization CNOT gate operating on photon $a1$ ($a2$) and photon b in the upper (lower) path. (b) Experimental setup. A pulsed ultraviolet (UV) laser is focused on two beta-barium borate (BBO) crystals and produces two photon pairs $a1$–$a2$ and b–t. By tuning HWP1 and QWP1, the first photon pair, $a1$–$a2$, is prepared at $\epsilon|H\rangle_{a1}|H\rangle_{a2} + \zeta|V\rangle_{a1}|V\rangle_{a2}$, which serves as the initial state of system A. BD1 and its surrounding waveplates (HWP2, QWP2, HWP3, QWP3, HWP4 and QWP4) prepare photon b at $\eta|H0\rangle_b + \kappa|H1\rangle_b + \lambda|V0\rangle_b + \mu|V1\rangle_b$, which serves as the initial state of system B. The two polarization CNOT gates based on PPBS are used to implement the optical CX_4 on system A and system B. BD2 and its surrounding waveplates (QWP5, HWP5, HWP at 0°, HWP at 45°, QWP6 and HWP6) are used to analyze the ququart state.

lower path. As a result, the desired CX_4 gate can be achieved by the two polarization CNOT gates as shown in Fig. 3(a).

Note that the use of two photons to encode the control qubit is mainly due to the following experimental considerations. The optical CNOT gates used experimentally are based on postselection measurements, and such CNOT gates would fail when they act on the same two photons twice in a row. By using two photons $a1$ and $a2$ to encode the control qubit, the two CNOT gates are not acting on the same two photons, thus avoiding this problem.

B. Experimental Setup

Figure 3(b) shows the experimental setup for implementing the two QIT schemes. Two photon pairs are generated by passing femtosecond-pulse UV laser through type-II beta-barium borate (BBO) crystals (see Appendix A). Photons $a1$ and $a2$ of the first pair are prepared at $\epsilon|H\rangle_{a1}|H\rangle_{a2} + \zeta|V\rangle_{a1}|V\rangle_{a2}$, which serves as the initial state of system A. By passing through the beam displacer BD1 and its surrounding waveplates (HWP2, QWP2, HWP3, QWP3, HWP4, and QWP4), photon b from the second pair is prepared at $\eta|H0\rangle_b + \kappa|H1\rangle_b + \lambda|V0\rangle_b + \mu|V1\rangle_b$, which serves as the initial state of system B. The upper (lower) rail of photon b is then superposed with photon $a1$ ($a2$) on a partial polarization beam-splitter (PPBS). The PPBS, the loss elements, and its surrounding half wave-plates can realize a polarization CNOT gate on photon $a1$ ($a2$) and photon b in the upper (lower) path [41]. These two polarization CNOT gates together realize a CX_4 gate on qubit A and ququart B (see Appendix C), and the state of the three photons becomes

$$\epsilon|H\rangle_{a1}|H\rangle_{a2} \otimes (\eta|H0\rangle_b + \kappa|H1\rangle_b + \lambda|V0\rangle_b + \mu|V1\rangle_b) + \zeta|V\rangle_{a1}|V\rangle_{a2} \otimes (\eta|V0\rangle_b + \kappa|V1\rangle_b + \lambda|H0\rangle_b + \mu|H1\rangle_b).$$

C. Results of the 4-to-2 QIT

To demonstrate the 4-to-2 QIT, ϵ and ζ are set to $1/\sqrt{2}$, and the three-photon state after the CX_4 gate can be written as

$$\frac{1}{\sqrt{2}}|H\rangle_{a1}|H\rangle_{a2} \otimes (\eta|H0\rangle_b + \kappa|H1\rangle_b + \lambda|V0\rangle_b + \mu|V1\rangle_b) + \frac{1}{\sqrt{2}}|V\rangle_{a1}|V\rangle_{a2} \otimes (\eta|V0\rangle_b + \kappa|V1\rangle_b + \lambda|H0\rangle_b + \mu|H1\rangle_b).$$

Active feed-forward is needed for a full, deterministic 4-to-2 QIT. However, in this proof-of-principle experiment, we did not apply feed-forward but used postselection to realize a probabilistic 4-to-2 QIT. By postselecting the $|H0\rangle_b$ and $|H1\rangle_b$ components and converting $|H0\rangle_b$ to $|H\rangle_b$ and $|H1\rangle_b$ to $|V\rangle_b$ using BD2 and its preceding waveplates, the three-photon state

$$\eta|H\rangle_{a1}|H\rangle_{a2}|H\rangle_b + \kappa|H\rangle_{a1}|H\rangle_{a2}|V\rangle_b + \lambda|V\rangle_{a1}|V\rangle_{a2}|H\rangle_b + \mu|V\rangle_{a1}|V\rangle_{a2}|V\rangle_b,$$

is obtained. By projecting photon $a2$ to $|D\rangle = \frac{1}{\sqrt{2}}(|H\rangle + |V\rangle)$, the two-photon state of $a1$ and b becomes

$$\eta|H\rangle_{a1}|H\rangle_b + \kappa|H\rangle_{a1}|V\rangle_b + \lambda|V\rangle_{a1}|H\rangle_b + \mu|V\rangle_{a1}|V\rangle_b.$$

The two qubits of quantum information originally concentrated on photon b are now distributed over two photons $a1$ and b, which indicates that one qubit of quantum information has been transferred from photon b to photon $a1$, thus achieving a 4-to-2 QIT.

We then measure the fidelity of the final state, $F = \mathrm{Tr}(\rho|\psi\rangle\langle\psi|)$, which is defined as the overlap between the ideal final state ($|\psi\rangle$) and the measured density matrix (ρ). The verification of the QIT results is based on fourfold coincidence detection which in our experiment occurs with a rate of

0.22 Hz. In each setting, the typical data collection time is 10 min, which allows us to sufficiently suppress Poisson noise.

Five different initial states of B are prepared for demonstrating the 4-to-2 QIT:

$$|\phi_1\rangle_B = \frac{1}{\sqrt{2}}(|\mathbf{0}\rangle_B + |\mathbf{1}\rangle_B) = \frac{1}{\sqrt{2}}(|H0\rangle_b + |H1\rangle_b),$$
$$|\phi_2\rangle_B = \frac{1}{\sqrt{2}}(|\mathbf{0}\rangle_B + |\mathbf{2}\rangle_B) = \frac{1}{\sqrt{2}}(|H0\rangle_b + |V0\rangle_b),$$
$$|\phi_3\rangle_B = \frac{1}{2}(|\mathbf{0}\rangle_B + |\mathbf{1}\rangle_B + |\mathbf{2}\rangle_B + |\mathbf{3}\rangle_B) = \frac{1}{2}(|H0\rangle_b + |H1\rangle_b + |V0\rangle_b + |V1\rangle_b),$$
$$|\phi_4\rangle_B = \frac{1}{\sqrt{2}}(|\mathbf{1}\rangle_B + |\mathbf{2}\rangle_B) = \frac{1}{\sqrt{2}}(|H1\rangle_b + |V0\rangle_b),$$
$$|\phi_5\rangle_B = \frac{1}{2}(|\mathbf{0}\rangle_B - |\mathbf{1}\rangle_B - |\mathbf{2}\rangle_B - |\mathbf{3}\rangle_B) = \frac{1}{2}(|H0\rangle_b - |H1\rangle_b - |V0\rangle_b - |V1\rangle_b).$$

Figures 4(a)–4(e) shows the 4-to-2 QIT results of the five different initial states on specific bases from which the fidelities can be extracted. For each of the five initial ququart states $|\phi_1\rangle_B$ to $|\phi_5\rangle_B$, the fidelity of the final state of A and B is, in numerical sequence: 0.8860 ± 0.0298, 0.7686 ± 0.0271, 0.7342 ± 0.0255, 0.7375 ± 0.0203, and 0.8220 ± 0.0164, which are summarized in Fig. 4(f). The fluctuation of the fidelities in the experiment stems from the fact that the realized CNOT gates have different performance for different control qubits, i.e., the noise is higher when the polarization of the control qubit is horizontal.

D. Results of the 2-to-4 QIT

To demonstrate the 2-to-4 QIT, λ and μ are set to zero, and the quantum state after the CX_4 gate can be written as

$$\epsilon|H\rangle_{a1}|H\rangle_{a2} \otimes (\eta|H0\rangle_b + \kappa|H1\rangle_b) + \zeta|V\rangle_{a1}|V\rangle_{a2} \otimes (\eta|V0\rangle_b + \kappa|V1\rangle_b).$$

By projecting both photons $a1$ and $a2$ to $|D\rangle$, the quantum state of photon b becomes

$$\epsilon\eta|H0\rangle_b + \epsilon\kappa|H1\rangle_b + \zeta\eta|V0\rangle_b + \zeta\kappa|V1\rangle_b.$$

This ququart state of photon b is then analyzed by the measurement setup consisting of BD2, its surrounding waveplates,

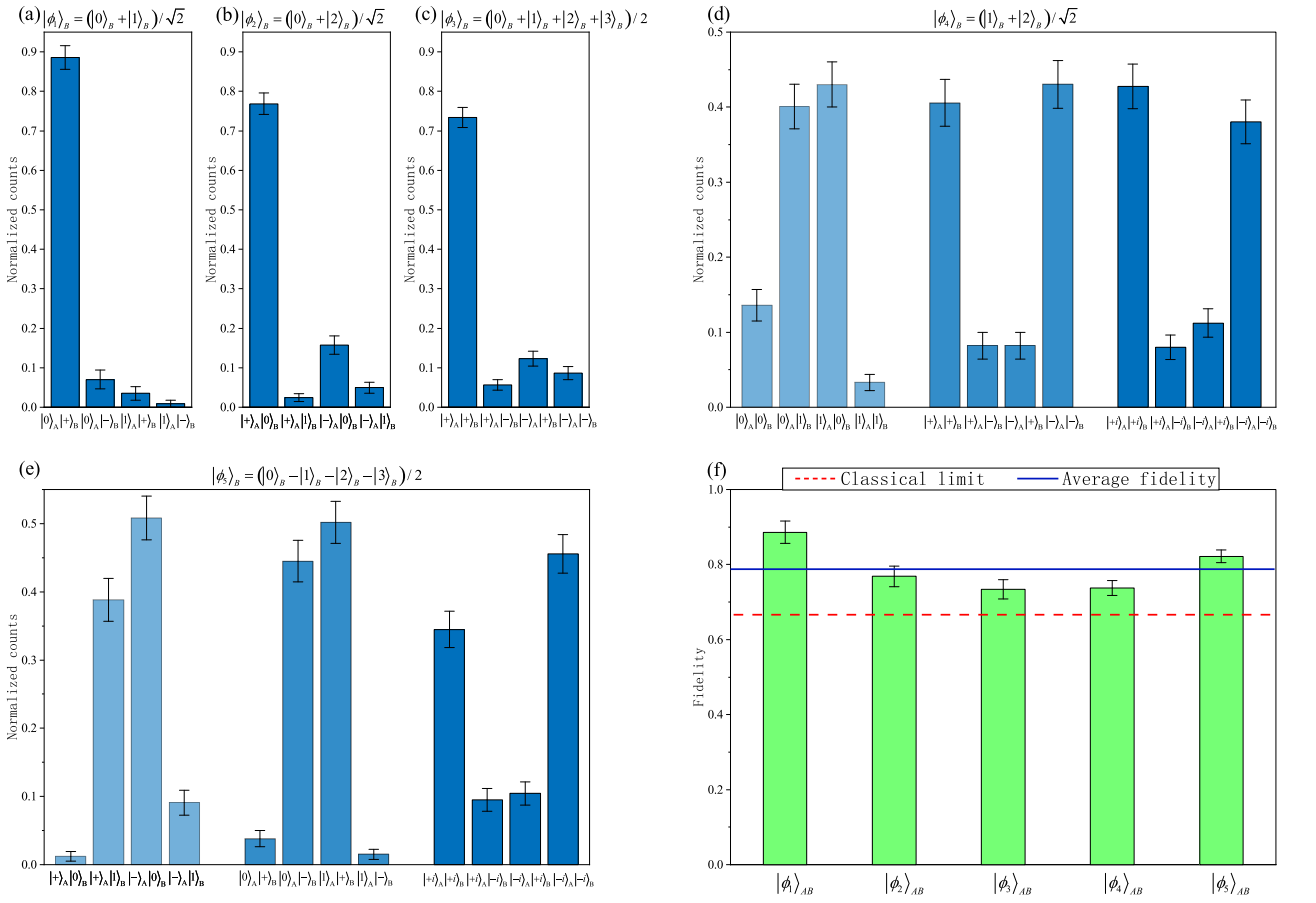

Fig. 4. Experimental results for the quantum information transfer from ququart B to qubit A. (a)–(e) Measurement results of the final state of A and B for the initial states $|\phi_1\rangle_B$, $|\phi_2\rangle_B$, …, and $|\phi_5\rangle_B$. Here $|\pm\rangle = \frac{1}{\sqrt{2}}(|0\rangle \pm |1\rangle)$ and $|\pm i\rangle = \frac{1}{\sqrt{2}}(|0\rangle \pm i|1\rangle)$. (f) Summary of the fidelities of the partial quantum state transfer for the five initial states. The average achieved fidelity of 0.7897 ± 0.0109 overcomes the classical bound of 2/3. The error bars (SD) are calculated according to propagated Poissonian counting statistics of the raw detection events.

the polarization beamsplitter (PBS), and the single-photon detector D3 (see Appendix D). The two qubits of quantum information originally distributed over system A (photons $a1$ and $a2$) and system B (photon b) are now concentrated on system B, which indicates that one qubit of quantum information has been transferred from system A to system B, thus achieving a 2-to-4 QIT.

Nine different initial states of A and B are used in the general quantum state transfer experiment:

$$
\begin{aligned}
|\psi_1\rangle_{AB} &= \frac{1}{\sqrt{2}}(|\mathbf{0}\rangle_A + i|\mathbf{1}\rangle_A) \otimes |\mathbf{0}\rangle_B \\
&= \frac{1}{\sqrt{2}}(|H\rangle_{a1}|H\rangle_{a2} + i|V\rangle_{a1}|V\rangle_{a2}) \otimes |H0\rangle_b, \\
|\psi_2\rangle_{AB} &= \frac{1}{\sqrt{2}}(|\mathbf{0}\rangle_A + i|\mathbf{1}\rangle_A) \otimes \frac{1}{\sqrt{2}}(|\mathbf{0}\rangle_B - |\mathbf{1}\rangle_B) \\
&= \frac{1}{\sqrt{2}}(|H\rangle_{a1}|H\rangle_{a2} + i|V\rangle_{a1}|V\rangle_{a2}) \\
&\quad \otimes \frac{1}{\sqrt{2}}(|H0\rangle_b - |H1\rangle_b), \\
|\psi_3\rangle_{AB} &= \frac{1}{\sqrt{2}}(|\mathbf{0}\rangle_A + i|\mathbf{1}\rangle_A) \otimes \frac{1}{\sqrt{2}}(|\mathbf{0}\rangle_B + i|\mathbf{1}\rangle_B) \\
&= \frac{1}{\sqrt{2}}(|H\rangle_{a1}|H\rangle_{a2} + i|V\rangle_{a1}|V\rangle_{a2}) \\
&\quad \otimes \frac{1}{\sqrt{2}}(|H0\rangle_b + i|H1\rangle_b), \\
|\psi_4\rangle_{AB} &= \frac{1}{\sqrt{2}}(|\mathbf{0}\rangle_A + |\mathbf{1}\rangle_A) \otimes |\mathbf{0}\rangle_B \\
&= \frac{1}{\sqrt{2}}(|H\rangle_{a1}|H\rangle_{a2} + |V\rangle_{a1}|V\rangle_{a2}) \otimes |H0\rangle_b, \\
|\psi_5\rangle_{AB} &= \frac{1}{\sqrt{2}}(|\mathbf{0}\rangle_A + |\mathbf{1}\rangle_A) \otimes \frac{1}{\sqrt{2}}(|\mathbf{0}\rangle_B + |\mathbf{1}\rangle_B) \\
&= \frac{1}{\sqrt{2}}(|H\rangle_{a1}|H\rangle_{a2} + |V\rangle_{a1}|V\rangle_{a2}) \\
&\quad \otimes \frac{1}{\sqrt{2}}(|H0\rangle_b + |H1\rangle_b), \\
|\psi_6\rangle_{AB} &= \frac{1}{\sqrt{2}}(|\mathbf{0}\rangle_A + |\mathbf{1}\rangle_A) \otimes \frac{1}{\sqrt{2}}(|\mathbf{0}\rangle_B - i|\mathbf{1}\rangle_B) \\
&= \frac{1}{\sqrt{2}}(|H\rangle_{a1}|H\rangle_{a2} + |V\rangle_{a1}|V\rangle_{a2}) \\
&\quad \otimes \frac{1}{\sqrt{2}}(|H0\rangle_b - i|H1\rangle_b), \\
|\psi_7\rangle_{AB} &= |\mathbf{1}\rangle_A \otimes |\mathbf{0}\rangle_B = |V\rangle_{a1}|V\rangle_{a2} \otimes |H0\rangle_b, \\
|\psi_8\rangle_{AB} &= |\mathbf{1}\rangle_A \otimes \frac{1}{\sqrt{2}}(|\mathbf{0}\rangle_B + |\mathbf{1}\rangle_B) \\
&= |V\rangle_{a1}|V\rangle_{a2} \otimes \frac{1}{\sqrt{2}}(|H0\rangle_b + |H1\rangle_b), \\
|\psi_9\rangle_{AB} &= |\mathbf{1}\rangle_A \otimes \frac{1}{\sqrt{2}}(|\mathbf{0}\rangle_B - i|\mathbf{1}\rangle_B) \\
&= |V\rangle_{a1}|V\rangle_{a2} \otimes \frac{1}{\sqrt{2}}(|H0\rangle_b - i|H1\rangle_b).
\end{aligned}
$$

Figures 5(a)–5(i) show the 2-to-4 QIT results of the nine different initial states on specific bases, from which the fidelities can be directly extracted. For each of the nine initial states $|\psi_1\rangle_{AB}$ to $|\psi_9\rangle_{AB}$, the fidelity of the final state of ququart B is, in numerical sequence: 0.8018 ± 0.0271, 0.7220 ± 0.0289, 0.6997 ± 0.0241, 0.8772 ± 0.0217, 0.7897 ± 0.0257, 0.8080 ± 0.0249, 0.8770 ± 0.0130, 0.8431 ± 0.0134, and 0.9171 ± 0.0138, which is summarized in Fig. 5(j).

The reported data are raw data without any background subtraction, and the main errors are due to double pair emission, imperfection in preparation of the initial states, and the nonideal interference at the PPBS and BD2. Throughout our experiments, whether 2-to-4 or 4-to-2, we are actually transmitting one qubit of quantum information. Specifically, in the 4-to-2 experiment, particle B is preloaded with two qubits of quantum information and sends one of two qubits to A. In the 2-to-4 experiment, the one qubit carried by A is transmitted to B which is already preloaded with one qubit of quantum information. Therefore, the classical threshold should be $2/(d+1) = 2/3$ in our experiments. Despite the experimental noise, the measured fidelities of the quantum states are all well above the classical limit $2/3$, defined as the optimal state-estimation fidelity on a single copy of a one-qubit system [42]. These results prove the successful realization of the 4-to-2 and the 2-to-4 QIT.

4. CONCLUSION

In this work, we have experimentally transferred one qubit of quantum information from a 4D photon preloaded with two qubits of quantum information to a 2D photon. We have also experimentally realized the inverse operation, namely transferring one qubit of quantum information from a 2D photon to a 4D photon preloaded with one qubit of quantum information. Our experiments show that quantum information is independent of its carriers and can be freely transferred between quantum objects of different dimensions. Although the present experiments are realized in the linear optical architecture, our protocols themselves are not limited to the optical system and can be applied to other quantum systems such as trapped atoms [19], ions [21,22], and electrons [23].

The techniques developed in this work for entangling operations on photons of different dimensions can be used to prepare a new type of maximally entangled state such as $1/2(|0\rangle_{a1}|0\rangle_{a2} \otimes |0\rangle_b + |0\rangle_{a1}|1\rangle_{a2} \otimes |1\rangle_b + |1\rangle_{a1}|0\rangle_{a2} \otimes |2\rangle_b + |1\rangle_{a1}|1\rangle_{a2} \otimes |3\rangle_b)$, where photons $a1$ and $a2$ are both 2D and belong to system A, and photon b is 4D and belongs to system B. System A and system B have the same dimension but a different number of particles. Such maximally entangled states with asymmetric particle numbers can be used as a physical resource for realizing quantum teleportation between systems with the same dimension but different particle numbers.

Our approach can be readily extended to higher dimensional cases (see Appendixes E and F). With these QIT operations, one can either concentrate the quantum information from multiple objects to one object or distribute the quantum information from one object to multiple objects. Such operations have the potential to simplify the construction of multiqubit

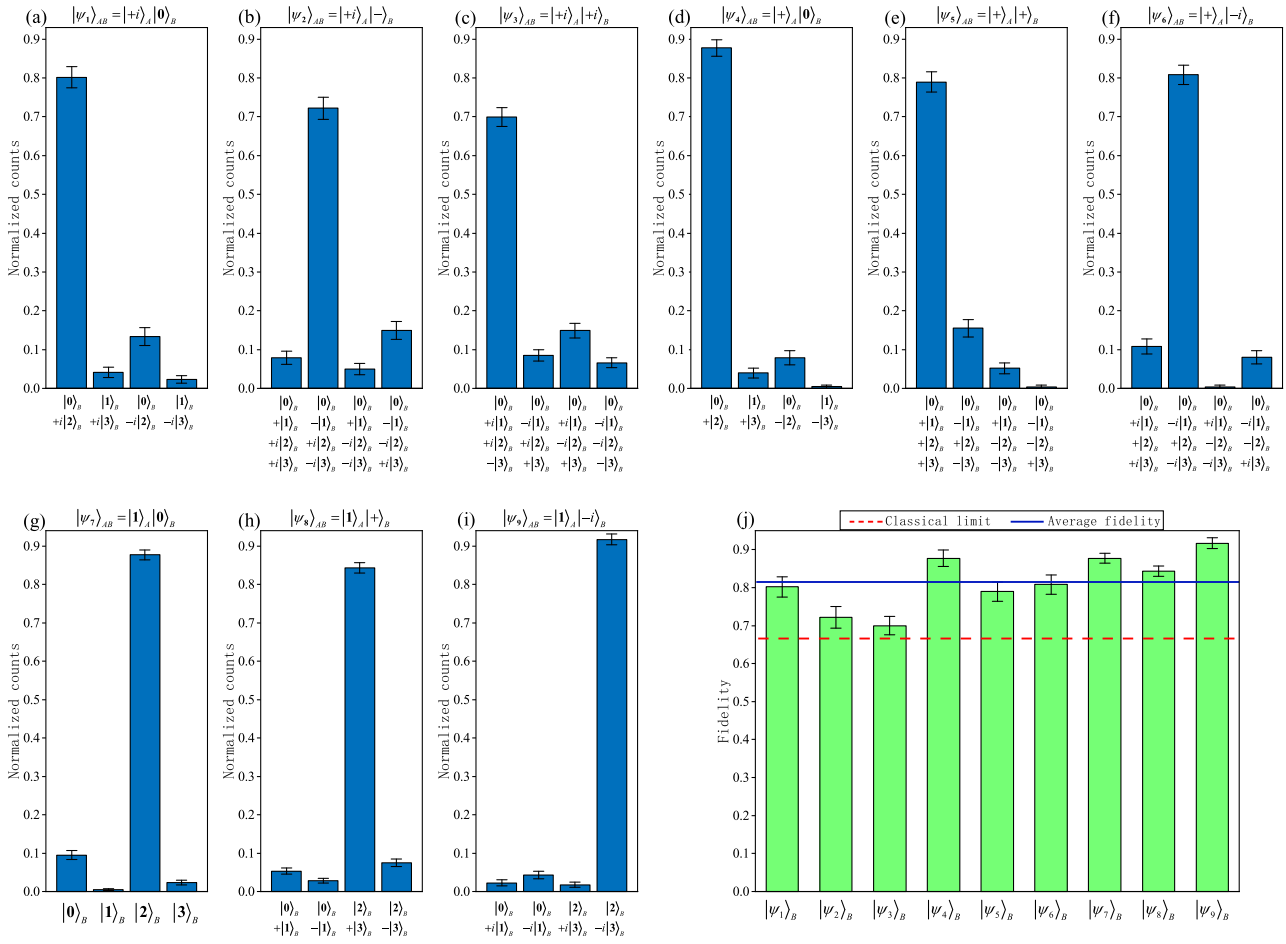

Fig. 5. Experimental results for the quantum information transfer from qubit A to ququart B. (a)–(i) Measurement results of the final state of B for the initial states $|\psi_1\rangle_{AB}$, $|\psi_2\rangle_{AB}$, …, and $|\psi_9\rangle_{AB}$. Here $|\pm\rangle = \frac{1}{\sqrt{2}}(|0\rangle \pm |1\rangle)$ and $|\pm i\rangle = \frac{1}{\sqrt{2}}(|0\rangle \pm i|1\rangle)$. (j) Summary of the fidelities of the general quantum state transfer for the nine initial states. The average achieved fidelity of 0.8151 ± 0.0074 overcomes the classical bound of 2/3. The error bars (SD) are calculated according to propagated Poissonian counting statistics of the raw detection events.

gates [43,44] (see Appendix G) and find applications in quantum computation and quantum simulations.

APPENDIX A: GENERATING TWO PHOTON PAIRS

For the sake of simplicity, in Fig. 3(b) of the main text, we only show a simplified version of the spontaneous parametric down-conversion (SPDC) sources. Figure 6 shows the detailed experimental setup for generating two photon pairs. An ultraviolet pulse laser centered at 390 nm is split into two parts, which are used to generate two SPDC photon pairs. The lower part of the laser directly pumps a BBO crystal to generate a pair of photons in the state $|V_b\rangle|H_t\rangle$ via beamlike type-II SPDC, where photon t is used for the trigger. The upper part of the laser goes through HWP1 and QWP1 to prepare its polarization at $\alpha|H\rangle + \beta|V\rangle$. It then passes through an arrangement of two beam displacers (BDs) and HWPs to separate the laser into two beams by 4 mm apart (such configuration was first adopted by Zhong *et al.* in Ref. [45]). The two beams then focus on a BBO crystal to generate two photon pairs in the states

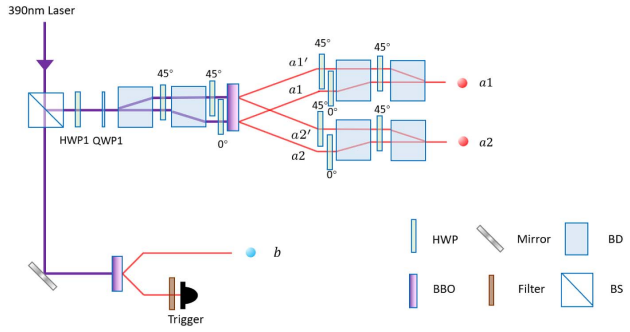

Fig. 6. Experimental setup for generating two photon pairs.

$|V_{a1}\rangle|H_{a2}\rangle$ and $|V_{a1'}\rangle|H_{a2'}\rangle$ via beamlike type-II SPDC, where the subscripts denote the spatial modes. $|V_{a1}\rangle|H_{a2}\rangle$ and $|V_{a1'}\rangle|H_{a2'}\rangle$ are then rotated using HWPs to $|H_{a1}\rangle|H_{a2}\rangle$ and $|V_{a1'}\rangle|V_{a2'}\rangle$, respectively. Photon pairs of $|H_{a1}\rangle|H_{a2}\rangle$ and $|V_{a1'}\rangle|V_{a2'}\rangle$ are then combined into the same spatial modes using two BDs. After tilting the two BDs to finely tune the relative phase between the two components,

the two photons $a1$ and $a2$ are prepared into $\alpha|H\rangle_{a1}|H\rangle_{a2}+\beta|V\rangle_{a1}|V\rangle_{a2}$, which is the desired quantum state of system A.

APPENDIX B: TWO-PHOTON INTERFERENCE ON A PPBS

The PPBS implements the quantum phase gate by reflecting vertically polarized light perfectly and reflecting (transmitting) 1/3 (2/3) of horizontally polarized light. To realize a perfect quantum gate with the PPBS, the input photons on the PPBS need to be indistinguishable to each other. To evaluate the indistinguishability of the input photons, a two-photon Hong-Ou-Mandel (HOM) interference on the PPBS needs to be measured. For large delay, the two photons are completely distinguishable due to their time of arrival. The probability to get a coincidence from an $|HH\rangle$ input is then 5/9. In case of perfectly indistinguishable photons at zero delay, the probability drops to 1/9. From the above considerations, the theoretical dip visibility $V_{\text{th}} = 80\%$ is obtained, which is defined via $V = (c_\infty - c_0)/c_0$, where c_0 is the count rate at zero delay, and c_∞ is the count rate for large delay. As shown in Fig. 7, the HOM interference is experimentally measured, and a dip visibility of $V_{\text{exp}} = 0.661 \pm 0.0015$ is obtained, where the error bar is calculated from the Poissonian counting statistics of the detection events. The overlap quality $Q = V_{\text{exp}}/V_{\text{th}} = 0.826 \pm 0.0019$ indicates that about 17.4% of the detected photon pairs are distinguishable.

APPENDIX C: IMPLEMENTATION OF CX_4 GATE USING LINEAR OPTICS

As described in the main text, an optical CX_4 gate between system A (photons $a1$ and $a2$) and system B (photon b) can be implemented with a setup as shown in Fig. 8(a). Photons $a1$ and $a2$ encode the control qubit, and its initial state is $\epsilon|\mathbf{0}\rangle_A + \zeta|\mathbf{1}\rangle_A = \epsilon|H\rangle_{a1}|H\rangle_{a2} + \zeta|V\rangle_{a1}|V\rangle_{a2}$. Photon b encodes the target ququart, and its initial state is $\eta|\mathbf{0}\rangle_B + \kappa|\mathbf{1}\rangle_B = \eta|H0\rangle_b + \kappa|H1\rangle_b$. After passing through the loss elements that transmit horizontally polarized light perfectly and transmit 1/3 of vertically polarized light, photon $a1$ ($a2$) and photon b in the upper (lower) mode are superposed on the PPBS. The PPBS, the loss elements, and the two surrounding HWPs at 22.5° together implement a polarization CNOT operation on the input photons [41,46,47]. Such optical circuit can thus realize the following transformations:

$$|H\rangle_{a1}|H\rangle_{a2} \otimes |H0\rangle_b \rightarrow |H\rangle_{a1}|H\rangle_{a2} \otimes |H0\rangle_b,$$
$$|H\rangle_{a1}|H\rangle_{a2} \otimes |H1\rangle_b \rightarrow |H\rangle_{a1}|H\rangle_{a2} \otimes |H1\rangle_b,$$
$$|V\rangle_{a1}|V\rangle_{a2} \otimes |H0\rangle_b \rightarrow |V\rangle_{a1}|V\rangle_{a2} \otimes |V0\rangle_b,$$
$$|V\rangle_{a1}|V\rangle_{a2} \otimes |H1\rangle_b \rightarrow |V\rangle_{a1}|V\rangle_{a2} \otimes |V1\rangle_b.$$

As a result, after passing through this optical circuit, the initial input state

$$(\epsilon|\mathbf{0}\rangle_A + \zeta|\mathbf{1}\rangle_A) \otimes (\eta|\mathbf{0}\rangle_B + \kappa|\mathbf{1}\rangle_B)$$
$$= (\epsilon|H\rangle_{a1}|H\rangle_{a2} + \zeta|V\rangle_{a1}|V\rangle_{a2}) \otimes (\eta|H0\rangle_b + \kappa|H1\rangle_b),$$

would become

$$\epsilon|H\rangle_{a1}|H\rangle_{a2} \otimes (\eta|H0\rangle_b + \kappa|H1\rangle_b)$$
$$+ \zeta|V\rangle_{a1}|V\rangle_{a2} \otimes (\eta|V0\rangle_b + \kappa|V1\rangle_b)$$
$$= \epsilon|\mathbf{0}\rangle_A \otimes (\eta|\mathbf{0}\rangle_B + \kappa|\mathbf{1}\rangle_B) + \zeta|\mathbf{1}\rangle_A \otimes (\eta|\mathbf{2}\rangle_B + \kappa|\mathbf{3}\rangle_B),$$

which is exactly the desired output state of a CX_4 gate. The above optical CX_4 gate operates with a success probability of 1/27. In practice, to combat low count rates, we adopt the method proposed in Ref. [41] to simplify the implementation of the optical CX_4 gate. The simplified experimental setup is shown in Fig. 8(b). We achieve a correct balance by removing the loss elements and prebiasing the input polarization states during gate characterization. The initial state of photons $a1$ and $a2$ is now prepared at

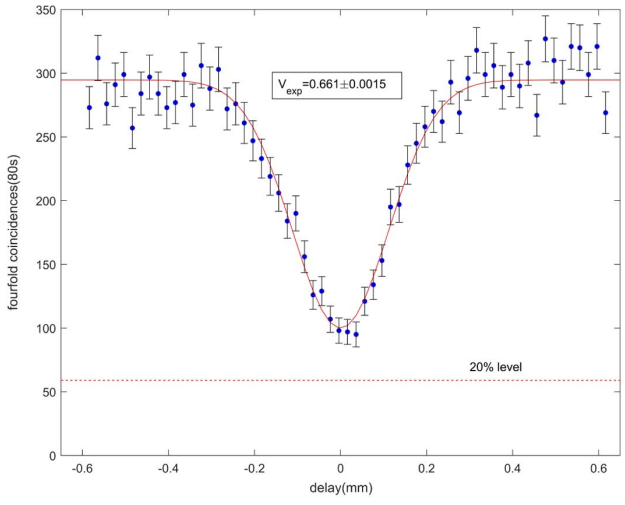

Fig. 7. HOM interference at the PPBS for an $|HH\rangle$ input. In case of perfect interference, the count rate should drop down to 20%, leading to a theoretically achievable dip visibility of 80%.

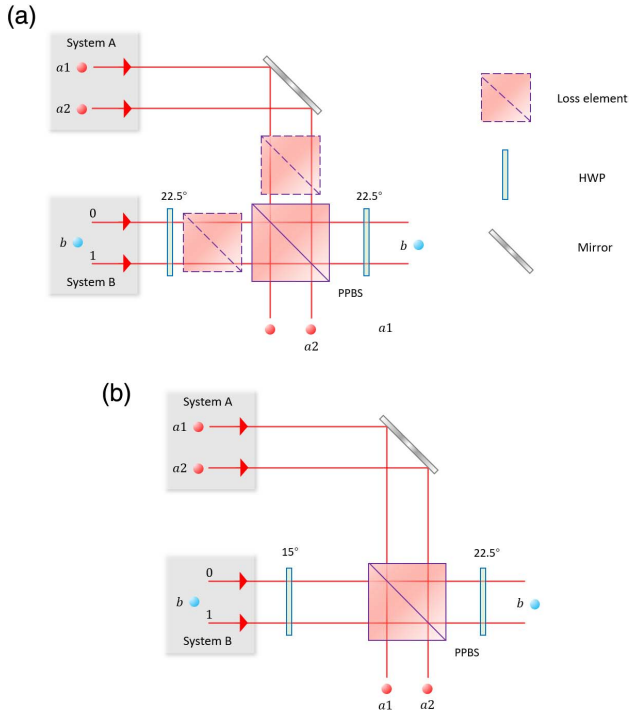

Fig. 8. CX_4 gate with linear optics. (a) The standard optical CX_4 gate. (b) The simplified optical CX_4 gate.

$\epsilon/\sqrt{|\epsilon|^2+\frac{|\zeta|^2}{9}}|H\rangle_{a1}|H\rangle_{a2}+(\zeta/3)/\sqrt{|\epsilon|^2+\frac{|\zeta|^2}{9}}|V\rangle_{a1}|V\rangle_{a2}$ instead of $\epsilon|H\rangle_{a1}|H\rangle_{a2}+\zeta|V\rangle_{a1}|V\rangle_{a2}$. The HWP applied on photon b before entering the PPBS is now set at 15°, thus converting photon b to the state $\sqrt{3}/2(\eta|H0\rangle+\kappa|H1\rangle)+1/2(\eta|V0\rangle+\kappa|V1\rangle)$ instead of $1/\sqrt{2}(\eta|H0\rangle+\kappa|H1\rangle)+1/\sqrt{2}(\eta|V0\rangle+\kappa|V1\rangle)$, which is the case if the HWP is set at 22.5°.

APPENDIX D: STATE ANALYSIS OF A PHOTONIC QUQUART STATE

A photon with both polarization and spatial degrees of freedom (DOFs) can encode a ququart state. To fully characterize such state, one needs to perform projective measurement onto various different ququart states. To fulfill this task, we build a ququart state analyzer as shown in Fig. 9, which can project the input ququart to any state in the form of $(a|H\rangle+b|V\rangle)\otimes(c|0\rangle+d|1\rangle)$. This setup works as follows. Suppose the input ququart state is $(a|H\rangle+b|V\rangle)\otimes(c|0\rangle+d|1\rangle)$. After passing through QWP3 and HWP3, which are used to convert $a|H\rangle+b|V\rangle$ to $|H\rangle$, the ququart state becomes $|H\rangle\otimes(c|0\rangle+d|1\rangle)$. The subsequent two HWPs (one at 45° and the other at 0°) and the BD are used to convert $|H\rangle\otimes(c|0\rangle+d|1\rangle)$ to $c|H\rangle+d|V\rangle$, which is now a polarization qubit state. QWP4 and HWP4 are then used to convert $c|H\rangle+d|V\rangle$ to $|H\rangle$, which can pass through the PBS and get detected by the SPD. As a result, for any input ququart state, only its $(a|H\rangle+b|V\rangle)\otimes(c|0\rangle+d|1\rangle)$ component can pass through the setup described above, which effectively realizes the desired projective measurement. By changing the parameters a, b, c, and d, this state analyzer can be used to perform a full state tomography on the input ququart state.

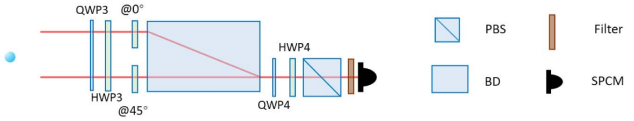

Fig. 9. State analyzer for a single-photon ququart state with both polarization and spatial degrees of freedom.

APPENDIX E: MERGE OPERATION

The scheme of 2-to-4 QIT can be extended to the higher dimensional case, i.e., transferring one qubit of unknown quantum information from a qubit to a qudit. We call the operation of aggregating quantum information from two particles to one particle the Merge operation, and Merge$(2,d\rightarrow 2d)$ denotes the aggregation of quantum information of a qubit and a d-dimensional qudit to a $2d$-dimensional qudit. The quantum circuit to implement Merge$(2,d\rightarrow 2d)$ is shown in Fig. 10(a), where the initial state of system A is $\alpha|\mathbf{0}\rangle_A+\beta|\mathbf{1}\rangle_A$, and the initial state of system B is $\sum_{i=0}^{d-1}\gamma_i|\boldsymbol{i}\rangle$, which is a d-dimensional qudit. A controlled-X_{2d} (CX_{2d}) gate is applied to A and B, where X_{2d} is a $2d$-dimensional unitary gate defined as $X_{2d}=\sum_{k=0}^{d-1}(|\boldsymbol{k}\rangle\langle\boldsymbol{k}+\boldsymbol{d}|+|\boldsymbol{k}+\boldsymbol{d}\rangle\langle\boldsymbol{k}|)$, which swaps $|\boldsymbol{k}\rangle$ and $|\boldsymbol{k}+\boldsymbol{d}\rangle$ for k in the range of 0 to $d-1$, expanding the state space of system B from d to $2d$ dimensions. The state of A and B is thus converted from

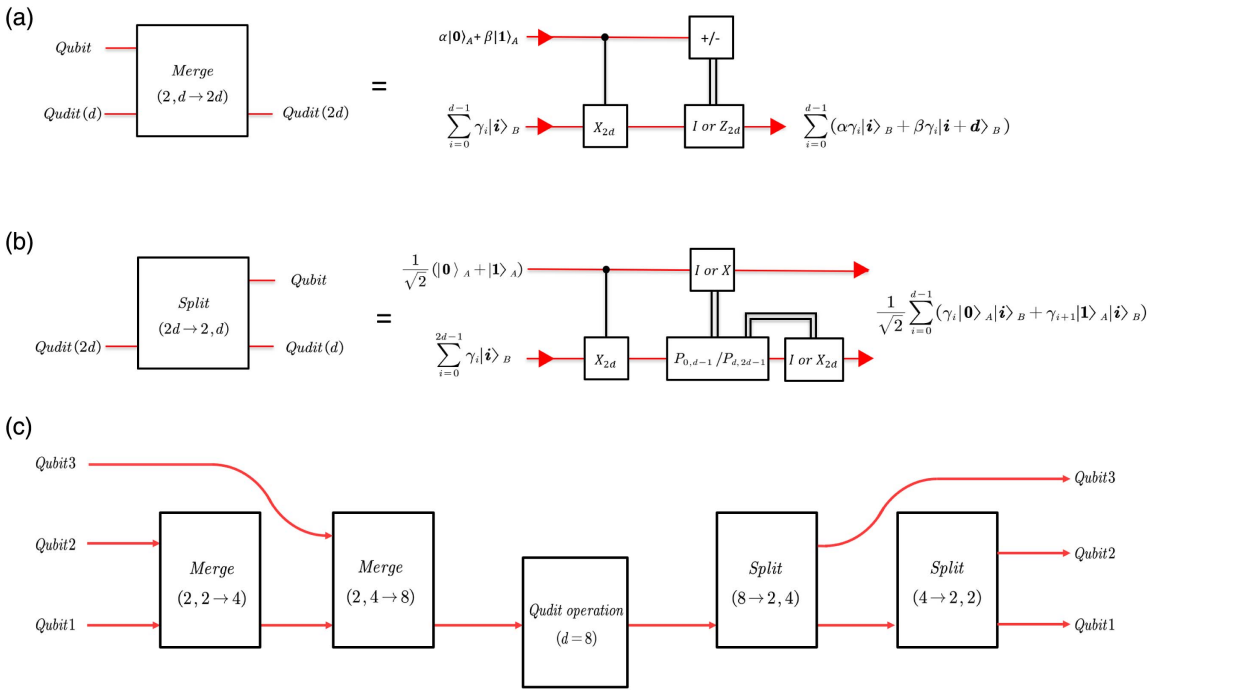

Fig. 10. (a) The Merge operation. The quantum circuit for merging the quantum information of a qubit and a d-dimensional qudit into a $2d$-dimensional qudit. (b) The Split operation. The quantum circuit for splitting the quantum information of a $2d$-dimensional qudit to a qubit and a d-dimensional qudit. (c) Implementing a three-qubit quantum gate using Merge and Split operations.

$$(\alpha|\mathbf{0}\rangle+\beta|\mathbf{1}\rangle)\otimes\sum_{i=0}^{d-1}\gamma_i|\boldsymbol{i}\rangle=\sum_{i=0}^{d-1}(\alpha\gamma_i|\mathbf{0}\rangle_A|\boldsymbol{i}\rangle_B+\beta\gamma_i|\mathbf{1}\rangle_A|\boldsymbol{i}\rangle_B) \tag{E1}$$

to

$$\begin{aligned}&\sum_{i=0}^{d-1}(\alpha\gamma_i|\mathbf{0}\rangle_A|\boldsymbol{i}\rangle_B+\beta\gamma_i|\mathbf{1}\rangle_A|\boldsymbol{i}+\boldsymbol{d}\rangle_B)\\&=|+\rangle_A\otimes\sum_{i=0}^{d-1}(\alpha\gamma_i|\boldsymbol{i}\rangle_B+\beta\gamma_i|\boldsymbol{i}+\boldsymbol{d}\rangle_B)\\&\quad+|-\rangle_B\otimes\sum_{i=0}^{d-1}(\alpha\gamma_i|\boldsymbol{i}\rangle_B-\beta\gamma_i|\boldsymbol{i}+\boldsymbol{d}\rangle_B).\end{aligned}$$

After measuring A in the $|\pm\rangle$ basis and forwarding the outcome to B, a $2d$-dimensional unitary operation (I_{2d} or Z_{2d}) is applied on B conditioned on the outcome and thus converts its state to

$$\sum_{i=0}^{d-1}(\alpha\gamma_i|\boldsymbol{i}\rangle_B+\beta\gamma_i|\boldsymbol{i}+\boldsymbol{d}\rangle_B), \tag{E2}$$

where

$$Z_{2d}=I_{2d}-2\sum_{k=0}^{d-1}|\boldsymbol{k}+\boldsymbol{d}\rangle\langle\boldsymbol{k}+\boldsymbol{d}|.$$

By comparing Eq. (E2) and Eq. (E1), one sees that the two quantum states have exactly the same form except for the difference in the state basis, which means that the quantum information originally stored in A and B has been merged into B.

APPENDIX F: SPLIT OPERATION

The scheme of 4-to-2 QIT can be extended to the higher dimensional case, i.e., transferring one qubit of unknown quantum information from a qudit to a qubit. We call this operation of distributing quantum information from one particle to two particles the Split operation, and Split($2d\to2, d$) denotes the distribution of quantum information from a $2d$-dimensional qudit to a qubit and a d-dimensional qudit. The quantum circuit to implement Split($2d\to2, d$) is shown in Fig. 10(b), where system A is initially in the state $\frac{1}{\sqrt{2}}(|\mathbf{0}\rangle_A+|\mathbf{1}\rangle_A)$, and the initial state of system B is in the $2d$-dimensional qudit state:

$$\sum_{\boldsymbol{i}=0}^{2d-1}\gamma_i|\boldsymbol{i}\rangle=\sum_{i=0}^{d-1}(\gamma_i|\boldsymbol{i}\rangle+\gamma_{i+d}|\boldsymbol{i}+\boldsymbol{d}\rangle). \tag{F1}$$

A CX_{2d} gate is applied to A and B, and their state becomes

$$\begin{aligned}&\frac{1}{\sqrt{2}}|\mathbf{0}\rangle\otimes\sum_{i=0}^{d-1}(\gamma_i|\boldsymbol{i}\rangle+\gamma_{i+d}|\boldsymbol{i}+\boldsymbol{d}\rangle)\\&\quad+\frac{1}{\sqrt{2}}|\mathbf{1}\rangle\otimes\sum_{i=0}^{d-1}(\gamma_i|\boldsymbol{i}+\boldsymbol{d}\rangle+\gamma_{i+d}|\boldsymbol{i}\rangle)\\&=\frac{1}{\sqrt{2}}\sum_{i=0}^{d-1}(\gamma_i|\mathbf{0}\rangle|\boldsymbol{i}\rangle+\gamma_{i+d}|\mathbf{1}\rangle|\boldsymbol{i}\rangle)\\&\quad+\frac{1}{\sqrt{2}}\sum_{i=0}^{d-1}(\gamma_i|\mathbf{1}\rangle|\boldsymbol{i}+\boldsymbol{d}\rangle+\gamma_{i+d}|\mathbf{0}\rangle|\boldsymbol{i}+\boldsymbol{d}\rangle).\end{aligned}$$

A projective measurement is then applied on B to measure whether it is in the subspace spanned by $|\mathbf{0}\rangle_B, |\mathbf{1}\rangle_B, \ldots, |\boldsymbol{d}-\mathbf{2}\rangle_B$, and $|\boldsymbol{d}-\mathbf{1}\rangle_B$ or the subspace spanned by $|\boldsymbol{d}\rangle_B$, $|\boldsymbol{d}+\mathbf{1}\rangle_B, \ldots, |\mathbf{2}\boldsymbol{d}-\mathbf{2}\rangle_B$, and $|\mathbf{2}\boldsymbol{d}-\mathbf{1}\rangle_B$. Based on the measurement outcome, unitary operations ($I\otimes I_{2d}$ or $X\otimes X_{2d}$) are applied on A and B, and their state becomes

$$\frac{1}{\sqrt{2}}\sum_{i=0}^{d-1}(\gamma_i|\mathbf{0}\rangle|\boldsymbol{i}\rangle+\gamma_{i+d}|\mathbf{1}\rangle|\boldsymbol{i}\rangle). \tag{F2}$$

Comparing Eq. (F2) and Eq. (F1), it is observed that the two quantum states have exactly the same form except for the difference in the state basis, which means that the quantum information originally stored in B is now split into A and B.

APPENDIX G: CONSTRUCTION OF MULTIQUBIT GATES

In various quantum information applications, including quantum computation and quantum simulation, multiqubit quantum gates are widely used. Theoretically, multiqubit quantum gates can be decomposed into two-qubit CNOT gates and single-qubit quantum gates for implementation, but in practice, such decomposition can be quite complex and consumes a lot of resources experimentally. Here, we propose a method to simplify the implementation of multiqubit quantum gates by using QIT methods. This approach essentially transforms an arbitrary n-qubit quantum gate operation into a unitary transform on a 2^n-dimensional qudit, which is simpler to implement in certain circumstances. For example, for a path-encoded 2^n-dimensional photon, when n is not very large, an arbitrary $2^n\times2^n$ qudit unitary transform can be readily implemented using the Reck scheme [48,49]. We present below our method using a 3-qubit quantum gate as an example. Specifically, the method can be divided into three steps. (1) The quantum information of the three input qubits is converged to a single particle, which can be achieved by two Merge operations. As shown in Fig. 10(c), a ququart is obtained by a Merge(2, $2\to4$) operation acting on qubit 2 and qubit 1. Then a Merge(2, $4\to8$) operation acts on qubit 3 and this ququart to obtain a qudit ($d=8$), which contains the quantum information of the input three qubits. (2) The qudit is then subjected to an 8×8 unitary transformation, which has the same mathematical form as the matrix of the three-qubit quantum gate expanded in the computational basis. (3) The quantum information of this qudit is then distributed to three particles, which can be achieved by two Split operations. The eight-dimensional qudit is split by a Split($8\to2,4$) operation to get a qubit and a ququart, and this ququart is then split by a Split($4\to2,2$) operation to finally get three qubits at the output, thus completing the three-qubit quantum gate. For an arbitrary n-qubit quantum gate, it is often simpler and more resource-efficient to use our method than the traditional decomposition of n-qubit quantum gates into CNOT gates and single-qubit quantum gates, as long as n is not very large, i.e., the 2^n-dimensional qudit can be easily unitary-transformed.

Funding. National Natural Science Foundation of China (61974168); Special Project for Research and Development

in Key Areas of Guangdong Province (2018B030329001, 2018B030325001); National Key Research and Development Program of China (2017YFA0305200, 2016YFA0301300).

Disclosures. The authors declare that there are no competing interests.

Data Availability. Data underlying the results presented in this paper are not publicly available at this time but may be obtained from the authors upon reasonable request.

†These authors contributed equally to this paper.

REFERENCES

1. W. Wootters and W. Zurek, "A single quantum cannot be cloned," Nature **299**, 802–803 (1982).
2. V. Scarani, S. Iblisdir, N. Gisin, and A. Acin, "Quantum cloning," Rev. Mod. Phys. **77**, 1225–1256 (2005).
3. C. H. Bennett, G. Brassard, C. Crépeau, R. Jozsa, A. Peres, and W. K. Wootters, "Teleporting an unknown quantum state via dual classical and Einstein-Podolsky-Rosen channels," Phys. Rev. Lett. **70**, 1895–1899 (1993).
4. S. Pirandola, J. Eisert, C. Weedbrook, A. Furusawa, and S. L. Braunstein, "Advances in quantum teleportation," Nat. Photonics **9**, 641–652 (2015).
5. J.-G. Ren, P. Xu, H. L. Yong, L. Zhang, S. K. Liao, J. Yin, W. Y. Liu, W. Q. Cai, M. Yang, L. Li, and K. X. Yang, "Ground-to-satellite quantum teleportation," Nature **549**, 70–73 (2017).
6. A. K. Ekert, "Quantum cryptography based on Bell's theorem," Phys. Rev. Lett. **67**, 661–663 (1991).
7. X. Ma, T. Herbst, T. Scheidl, D. Wang, S. Kropatschek, W. Naylor, B. Wittmann, A. Mech, J. Kofler, E. Anisimova, and V. Makarov, "Quantum teleportation over 143 kilometres using active feed-forward," Nature **489**, 269–273 (2012).
8. H. J. Kimble, "The quantum internet," Nature **453**, 1023–1030 (2008).
9. C. Simon, "Towards a global quantum network," Nat. Photonics **11**, 678–680 (2017).
10. R. Raussendorf and H. J. Briegel, "A one-way quantum computer," Phys. Rev. Lett. **86**, 5188–5191 (2001).
11. R. Raussendorf, D. E. Browne, and H. J. Briegel, "Measurement-based quantum computation on cluster states," Phys. Rev. A **68**, 022312 (2003).
12. P. Walther, K. J. Resch, T. Rudolph, E. Schenck, H. Weinfurter, V. Vedral, M. Aspelmeyer, and A. Zeilinger, "Experimental one-way quantum computing," Nature **434**, 169–176 (2005).
13. C. Reimer, S. Sciara, P. Roztocki, M. Islam, L. Romero Cortés, Y. Zhang, B. Fischer, S. Loranger, R. Kashyap, A. Cino, and S. T. Chu, "High-dimensional one-way quantum processing implemented on d-level cluster states," Nat. Phys. **15**, 148–153 (2019).
14. D. Gottesman and I. L. Chuang, "Demonstrating the viability of universal quantum computation using teleportation and single-qubit operations," Nature **402**, 390–392 (1999).
15. Y. P. Kandel, H. Qiao, S. Fallahi, G. C. Gardner, M. J. Manfra, and J. M. Nichol, "Coherent spin-state transfer via Heisenberg exchange," Nature **573**, 553–557 (2019).
16. Y. He, Y. M. He, Y. J. Wei, X. Jiang, K. Chen, C. Y. Lu, J. W. Pan, C. Schneider, M. Kamp, and S. Höfling, "Quantum state transfer from a single photon to a distant quantum-dot electron spin," Phys. Rev. Lett. **119**, 060501 (2017).
17. D. Bouwmeester, J. W. Pan, K. Mattle, M. Eibl, H. Weinfurter, and A. Zeilinger, "Experimental quantum teleportation," Nature **390**, 575–579 (1997).
18. A. Furusawa, J. L. Sørensen, S. L. Braunstein, C. A. Fuchs, H. J. Kimble, and E. S. Polzik, "Unconditional quantum teleportation," Science **282**, 706–709 (1998).
19. X.-H. Bao, X. F. Xu, C. M. Li, Z. S. Yuan, C. Y. Lu, and J. W. Pan, "Quantum teleportation between remote atomic-ensemble quantum memories," Proc. Natl. Acad. Sci. USA **109**, 20347–20351 (2012).
20. J. Sherson, H. Krauter, R. Olsson, B. Julsgaard, K. Hammerer, I. Cirac, and E. S. Polzik, "Quantum teleportation between light and matter," Nature **443**, 557–560 (2006).
21. M. Riebe, H. Häffner, C. F. Roos, W. Hänsel, J. Benhelm, G. P. T. Lancaster, T. W. Körber, C. Becher, F. Schmidt-Kaler, D. F. V. James, and R. Blatt, "Deterministic quantum teleportation with atoms," Nature **429**, 734–737 (2004).
22. M. D. Barrett, J. Chiaverini, T. Schaetz, J. Britton, W. M. Itano, J. D. Jost, E. Knill, C. Langer, D. Leibfried, R. Ozeri, and D. J. Wineland, "Deterministic quantum teleportation of atomic qubits," Nature **429**, 737–739 (2004).
23. H. Qiao, Y. P. Kandel, S. K. Manikandan, A. N. Jordan, S. Fallahi, G. C. Gardner, M. J. Manfra, and J. M. Nichol, "Conditional teleportation of quantum-dot spin states," Nat. Commun. **11**, 1 (2020).
24. W. Pfaff, B. J. Hensen, H. Bernien, S. B. van Dam, M. S. Blok, T. H. Taminiau, M. J. Tiggelman, R. N. Schouten, M. Markham, D. J. Twitchen, and R. Hanson, "Unconditional quantum teleportation between distant solid-state quantum bits," Science **345**, 532–535 (2014).
25. N. Fiaschi, B. Hensen, A. Wallucks, R. Benevides, J. Li, T. P. M. Alegre, and S. Gröblacher, "Optomechanical quantum teleportation," Nat. Photonics **15**, 817–821 (2021).
26. L. Steffen, Y. Salathe, M. Oppliger, P. Kurpiers, M. Baur, C. Lang, C. Eichler, G. Puebla-Hellmann, A. Fedorov, and A. Wallraff, "Deterministic quantum teleportation with feed-forward in a solid state system," Nature **500**, 319–322 (2013).
27. M. S. Blok, V. V. Ramasesh, T. Schuster, K. O'Brien, J. M. Kreikebaum, D. Dahlen, A. Morvan, B. Yoshida, N. Y. Yao, and I. Siddiqi, "Quantum information scrambling on a superconducting qutrit processor," Phys. Rev. X **11**, 021010 (2021).
28. Z. Zhao, Y. A. Chen, A. N. Zhang, T. Yang, H. J. Briegel, and J. W. Pan, "Experimental demonstration of five-photon entanglement and open-destination teleportation," Nature **430**, 54–58 (2004).
29. A. Barasinski, A. Černoch, and K. Lemr, "Demonstration of controlled quantum teleportation for discrete variables on linear optical devices," Phys. Rev. Lett. **122**, 170501 (2019).
30. Q. Zhang, A. Goebel, C. Wagenknecht, Y. A. Chen, B. Zhao, T. Yang, A. Mair, J. Schmiedmayer, and J. W. Pan, "Experimental quantum teleportation of a two-qubit composite system," Nat. Phys. **2**, 678–682 (2006).
31. X. Hu, C. Zhang, B. H. Liu, Y. F. Huang, C. F. Li, and G. C. Guo, "Experimental multi-level quantum teleportation," arXiv:1904.12249 (2019).
32. Y. Luo, H. S. Zhong, M. Erhard, X. L. Wang, L. C. Peng, M. Krenn, X. Jiang, L. Li, N. L. Liu, C. Y. Lu, and A. Zeilinger, "Quantum teleportation in high dimensions," Phys. Rev. Lett. **123**, 070505 (2019).
33. X. Wang, X. D. Cai, Z. E. Su, M. C. Chen, D. Wu, L. Li, N. L. Liu, C. Y. Lu, and J. W. Pan, "Quantum teleportation of multiple degrees of freedom of a single photon," Nature **518**, 516–519 (2015).
34. M. A. Nielsen and I. L. Chuang, *Quantum Computation and Quantum Information* (Cambridge University, 2000).
35. A. Barenco, C. H. Bennett, R. Cleve, D. P. DiVincenzo, N. Margolus, P. Shor, T. Sleator, J. A. Smolin, and H. Weinfurter, "Elementary gates for quantum computation," Phys. Rev. A **52**, 3457–3467 (1995).
36. G. Vidal and C. M. Dawson, "Universal quantum circuit for two-qubit transformations with three controlled-NOT gates," Phys. Rev. A **69**, 010301 (2004).
37. J. L. O'Brien, G. J. Pryde, A. G. White, T. C. Ralph, and D. Branning, "Demonstration of an all-optical quantum controlled-NOT gate," Nature **426**, 264–267 (2003).
38. K. S. Chou, J. Z. Blumoff, C. S. Wang, P. C. Reinhold, C. J. Axline, Y. Y. Gao, L. Frunzio, M. H. Devoret, L. Jiang, and R. J. Schoelkopf, "Deterministic teleportation of a quantum gate between two logical qubits," Nature **561**, 368–373 (2018).
39. A. Fedorov, L. Steffen, M. Baur, M. P. da Silva, and A. Wallraff, "Implementation of a Toffoli gate with superconducting circuits," Nature **481**, 170–172 (2012).

40. M. D. Reed, L. DiCarlo, S. E. Nigg, L. Sun, L. Frunzio, S. M. Girvin, and R. J. Schoelkopf, "Realization of three-qubit quantum error correction with superconducting circuits," Nature **482**, 382–385 (2012).
41. R. Okamoto, H. F. Hofmann, S. Takeuchi, and K. Sasaki, "Demonstration of an optical quantum controlled-NOT gate without path interference," Phys. Rev. Lett. **95**, 210506 (2005).
42. S. Massar and S. Popescu, "Optimal extraction of information from finite quantum ensembles," Phys. Rev. Lett. **74**, 1259–1263 (1995).
43. T. C. Ralph, K. J. Resch, and A. Gilchrist, "Efficient Toffoli gates using qudits," Phys. Rev. A **75**, 022313 (2007).
44. B. P. Lanyon, M. Barbieri, M. P. Almeida, T. Jennewein, T. C. Ralph, K. J. Resch, G. J. Pryde, J. L. O'brien, A. Gilchrist, and A. G. White, "Simplifying quantum logic using higher-dimensional Hilbert spaces," Nat. Phys. **5**, 134–140 (2009).
45. H. S. Zhong, Y. Li, W. Li, L. C. Peng, Z. E. Su, Y. Hu, Y. M. He, X. Ding, W. Zhang, H. Li, and L. Zhang, "12-photon entanglement and scalable scattershot boson sampling with optimal entangled-photon pairs from parametric down-conversion," Phys. Rev. Lett. **121**, 250505 (2018).
46. N. K. Langford, T. J. Weinhold, R. Prevedel, K. J. Resch, A. Gilchrist, J. L. O'Brien, G. J. Pryde, and A. G. White, "Demonstration of a simple entangling optical gate and its use in Bell-state analysis," Phys. Rev. Lett. **95**, 210504 (2005).
47. N. Kiesel, C. Schmid, U. Weber, R. Ursin, and H. Weinfurter, "Linear optics controlled-phase gate made simple," Phys. Rev. Lett. **95**, 210505 (2005).
48. M. Reck, A. Zeilinger, H. J. Bernstein, and P. Bertani, "Experimental realization of any discrete unitary operator," Phys. Rev. Lett. **73**, 58–61 (1994).
49. W. R. Clements, P. C. Humphreys, B. J. Metcalf, W. S. Kolthammer, and I. A. Walmsley, "Optimal design for universal multiport interferometers," Optica **3**, 1460–1465 (2016).